Structural, optical and electrical properties of a Schottky diode fabricated on Ce doped ZnO nanorods grown using a two step chemical bath deposition

MAM Ahmed[⊠a,b], WE Meyer[a], JM Nel[a]

[a]*Department of Physics, University of Pretoria, Private Bag X20, 0028 Hatfield, South Africa*
[b]*Department of Physics, Faculty of Education, University of Khartoum, P.O Box 461, Omdurman, Sudan*

Abstract

Schottky diodes based on pure and Ce doped ZnO nanorods with Ce at% from 0.0 to 10.0 were fabricated using a chemical bath deposition technique. The effect of Ce doping on structural, optical and electrical properties was studied. X-ray diffraction spectroscopy and field emission scanning electron microscopy were used to study the crystalline structure and surface morphology, respectively. Raman spectroscopy at room temperature revealed that the dominant $E_2(high)$ peaks of Ce doped ZnO nanorods were red shifted compared to those in undoped ZnO. Room temperature photoluminescence spectroscopy of as-synthesized pure and Ce-doped ZnO nanorods showed that the UV emission was also red shifted with Ce doping enhancing the green-yellow emission compared to undoped ZnO nanorods. The optical band gap of pure and Ce doped ZnO nanorods were obtained from UV-vis results. Moreover, the *I-V* characteristics of a fabricated Schottky diodes revealed that the rectification behaviour of the diodes was improved by Ce doping. The maximum rectification was obtained at 10.0 at% Ce with ideality factor of 1.34 and barrier height of 0.856 eV.

Keywords: ZnO, Chemical deposition, Structural properties, Optical properties, Electrical properties.

1. Introduction

In the last few decades, nanomatrials such as nanowires, nanotubes and nanorods have been the subject of study by many researchers due to their potential use in a wide range of devices such as transistors, photodiodes and sensing applications. Among these nanomaterials, metal oxides have found considerable interest owing to their chemical, sensing, photo-detection, piezoelectricity properties [1].

Synthesis and characterization of one-dimensional (1D) semiconductor materials have recently attracted more interest due to their physical properties that enable them to play a major role in optoelectronic and nanoscale electronic devices [2, 3, 4]. 1D zinc oxide-based (ZnO) material shows unique properties for technological applications, such as UV laser devices [5], chemical sensors [6], solar cells [7], acoustic and luminescent devices [8]. ZnO is a wide band gap (3.37 eV) semiconductor that is suitable for short wavelength optoelectronic applications. In addition, its high exciton binding energy (60 meV) allows excitonic emission at room temperature with high efficiency. The structural, optical and electrical properties of ZnO can be altered by doping with different elements. Because of its wide band gap energy, ZnO can be used as a host lattice for doping different elements such as transition and rare earth (RE) metals. Many reports are available on doping ZnO with metals such as Nd [9], Ag [10, 11], Ga [12, 13], Mn [14, 15] and Al [16, 17]. Furthermore, ZnO has attracted extensive interest in device fabrication.

Growth of ZnO nanostructures can be achieved by different techniques such as metal organic chemical vapour deposition [18], vapour-liquid-solid method [4], thermal evaporation [19], radiofrequency magnetron sputtering [20], pulsed laser deposition [21], spray pyrolysis [22] and epitaxial electrodeposition [23]. These techniques have been successfully used to produce highly oriented ZnO nanorods. However, many of these require reaction conditions such as high temperature and pressure which result in preventing large-scale production of these nanomaterials. On the

Email address: mustafa.sonbl@gmail.com (MAM Ahmed[⊠])

other hand, chemical solution processes greatly facilitate the fabrication of well aligned ZnO nanorods on a large scale at relatively low temperature. Among the chemical solution methods, chemical bath deposition (CBD) was adopted for this study due to its low cost, simple experimental setup and low temperature growth.

In order to improve the structural, optical and electrical properties of ZnO, doping with RE will be attractive due to the availability of 4f orbital [24]. RE ions are substantially used in different host materials as activators due to their high fluorescence efficiencies and narrow fluorescence bands. There are numerous reports on RE element doping of ZnO including doping with Sm [25, 26], Eu [27, 28, 29], Yb, Er, and La [30, 31]. Among the RE metals, Ce doping has attracted much attention because of it is unique properties: for examples (1) the redox couple Ce^{3+}/Ce^{4+} that allows the oxidized cerium to shift between CeO_2 and Ce_2O_3 under oxidizing conditions, (2) control over modifying the morphological properties of the host and (3) easy formation of oxygen vacancies [32]. Doping ZnO with Ce exhibited adaptable properties and have been studied extensively [32, 33, 34, 35]. Ge et al., [36] and Dar et al., [37] reported gas sensing properties of Ce doped ZnO, Yousefi and co-workers [38] studied photoelectrochemical activity, and Elisa et al. [39] reported photocatalytic activity of Ce doped ZnO. To the best of our knowledge there is no available report on fabricated Schottky diodes based on Ce doped ZnO nanorods prepared by CBD.

In this study, the CBD technique at low temperature (90° C) was used to fabricate Schottky diodes based on pure and Ce doped ZnO nanorods on an indium tin oxide substrate (ITO). The ITO substrate was used because of its transparency and conductivity. The structural, optical and electrical properties of Schottky diodes fabricated on pure and Ce doped ZnO nanorods were studied in detail. The pure and Ce doped ZnO nanorod structures shows rectification behaviour and the electrical parameters of the fabricated Schottky diodes are discussed.

2. Experimental methods

2.1. Materials

In these experiments the following materials were used as received without any further purification: zinc acetate dihydrate (98%, Merck), ethanol (99.95%, Merck), monoethanolamine (MEA) (98%, Merck), hexamethylenetetramine (HMTA) (99.5%, Sigma Aldrich), zinc nitrate hexahydrate (98%, Sigma Aldrich) and cerium nitrate hexahydrate (99.999%, Sigma Aldrich).

2.2. Deposition of the seed layer

A zinc oxide seed layer solution was prepared by dissolving zinc acetate in ethanol which was stirred for 1 h at 500 rpm and 60° C. Thereafter, MEA was added drop-wise to the solution as stabilizer while continuously stirring for 1 h under the same conditions. The molar ratio between zinc acetate and MEA was kept at 1:1. The clear, transparent solution was then aged for 72 h to increase its viscosity. Prior to the deposition, ITO substrates were cleaned with deionized water, ethanol, acetone and deionized water, in this order for 15 min each using an ultrasonic bath, and finally blown dry with nitrogen gas. The zinc oxide seed layer was spin coated on pre-cleaned ITO substrates three times at 3000 rpm for 30 s, thereafter, dried in an oven preheated at 90° C for 5 min. Finally, coated substrates were annealed at 150° C for 15 min to remove the residual solvents before growing the nanorods.

2.3. Deposition of the nanorods

For the fabrication of the ZnO nanorods, zinc nitrate hexahydrate and HMTA were dissolved in deionized water separately, stirred for 10 min and finally mixed together. The resulting milky solution was then placed in a water bath preheated to 90° C which was maintained throughout the deposition. ITO substrates seeded with undoped ZnO were immersed into the solution in such way the seeded side faced downward for 2 hrs. For Ce doped ZnO nanorods, different amounts of cerium nitrate hexahydrate (0, 2, 4, 6, 8 and 10 at% Ce) were dissolved in deionised water and stirred for 10 min and thereafter added to the mixture of zinc nitrate and HMTA with continuous stirring for 10 min to make sure homogeneous solutions were obtained. Finally, substrates were rinsed with deionized water several times to remove the residuals and blown dry with nitrogen gas, whereafter samples were kept in a closed container for further characterization. The results for sample doped at 2.0 at% Ce are not presented in this report because results are identical to undoped sample.

2.4. Fabrication of the Schottky contacts

Circular Pd contacts for electrical measurements were evaporated resistively onto the nanorods using a mechanical shadow mask. The Pd was deposited in a vacuum chmaber at The pressure in the chamber 5.5×10^{-6} mbar at rate of 0.1 nm/s to a thickness of 100 nm. Hence, Pd/ZnO/ITO and Pd/Ce-ZnO/ITO devices were fabricated.

3. Characterization

As-synthesized samples were characterized in terms of their surface morphology, elemental analysis and structure with a Zeiss Ultra Plus Field Emission Scanning Electron Microscopy (FESEM) integrated with energy dispersive X-ray spectroscopy (EDX) and X-ray diffraction (XRD) on a Bruker D8 ADVANCE machine (λ = 1.5406 nm), respectively. Room temperature Raman spectroscopy in the range 100 - 1500 nm was measured using WITec alpha 300R confocal Raman microscopy (high-resolution confocal Raman imaging) with excitation wavelength λ = 532 nm. A Cary Eclipse fluorescence spectrometer (λ = 344 nm) was used to study the photoluminescence of the as-synthesized samples in the range 350 - 800 nm. Varian Cary 100 UV-vis spectrometer was used to measure the optical transmittance of the as-synthesized samples at room temperature. Prior to the UV-vis measurements, the background was taken using a pre-cleaned blank ITO coated glass substrate. Finally, electrical measurements on fabricated Schottky diodes on pure and Ce doped ZnO nanorods at room temperature were performed using SMU (key sight B2912A) Keithely 230 meter.

4. Results and discussion

4.1. Structural and morphological results

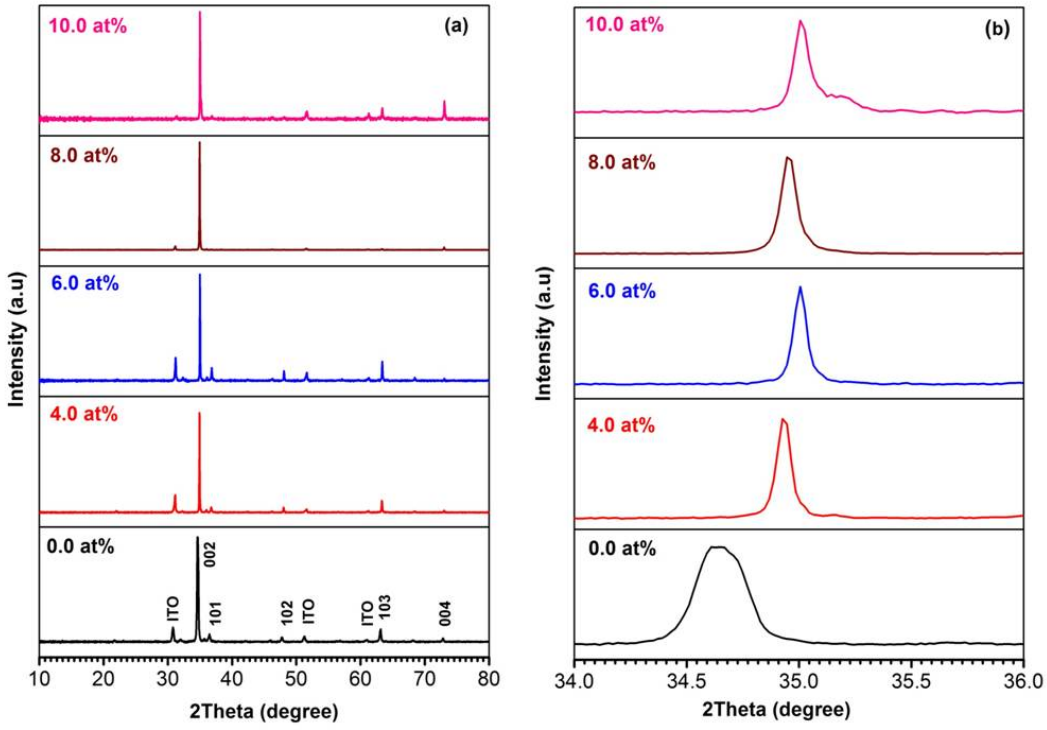

Figure 1: Room temperature XRD pattern of pure and Ce doped ZnO nanorods from bottom to top : (a) 0.0 to 10.0 at% and (b) is an enlargement of the (002) peak.

Table 1: Lattice parameters, peak position (2θ), FWHM, particle size (D), dislocation density (δ), unit cell volume (V) and Zn - O bond length (L) of as-synthesized samples.

Samples	Lattice parameter (Å)		2θ	FWHM (degree)	D (nm)	$\delta \times 10^{-4}$	V	L
at%	a	c	(degree)	(002)	(002)	(nm^{-2})	($Å^3$)	(Å)
0.00	3.229	5.176	34.648	0.252	34.46	8.324	46.46	1.961
4.00	3.203	5.133	34.926	0.079	110.15	0.975	45.57	1.949
6.00	3.188	5.123	35.000	0.072	120.88	0.821	45.50	1.941
8.00	3.188	5.130	34.946	0.086	100.38	1.183	45.69	1.940
10.00	3.196	5.123	35.000	0.069	126.14	0.748	45.30	1.944

Fig. 1 shows the XRD patterns of undoped and Ce doped ZnO nanorods measured at room temperature. All the peaks in the XRD patterns are assigned to the wurtzite structure of ZnO and the ITO substrates. Obtained XRD patterns are similar to the previously reported Ce doped ZnO nanorods [40]. As it can be seen in Fig. 1a, the as-synthesized samples have preferred orientation along the reflection plane (002). This indicates that the nanorods were grown perpendicular to the ITO substrates. The presence of the sharp peak in the XRD patterns of as-synthesized samples indicates that undoped and Ce doped ZnO nanorods were highly crystalline. The absence of Ce, CeO_2 and Ce_2O_3 peaks in the XRD spectrum emphasized that the Ce^{+3}/Ce^{+4} has substituted the Zn^{+2} and successfully incorporated into the ZnO lattice which inturn confirmed that the concentration of Ce dopant in ZnO was below the solubility limit. Moreover, the XRD pattern revealed that there is a shift in (002) peak position towards higher 2θ when compared to pure ZnO (see Table 1). Fig. 1b shows the shift of the (002) peak to higher 2θ values when Ce concentration is increased. This shift could be due the larger Ce^{+3}/Ce^{+4} ionic radius of 1.03 Å/0.92 Å compared to that of Zn^{+2} 0.74 Å which may be influenced the ZnO lattice. As can be observed from Fig. 1b, that the shift of the 2θ is not in a regular order. This could be attributed to the replacement of the Zn^{+2} by Ce^{+3}/Ce^{+4}. This shift in the (002) peak position agrees with the reported Ce doped ZnO nanorods [41, 35]. Table 1 summarizes the crystallographic properties of both ZnO and Ce doped ZnO samples. The calculated lattice parameters for undoped ZnO nanorods are in good agreement with JCPDF # 790205. The calculated lattice parameters for Ce doped samples decreased with increasing the Ce concentration compared to undoped samples. This decrease in the lattice parameters could be due to the effect of Ce dopant on ZnO lattice.

The average crystallite size (D) of as-synthesized samples calculated from Scherrer's equation [42], and the unit volume of the cell [43] are also shown in Table 1 together with FWHM of the (002) peak. The FWHM of (002) peak was found to decrease with increasing Ce dopant concentration indicating that the as-synthesized samples were of good quality. The calculated crystallite size was found to increase upon increasing the Ce dopant concentration when compared with undoped sample. The dislocation density (δ) of as-synthesized samples calculated from [44] was also found to decrease with increasing Ce dopant indicating that good quality samples were prepared. Furthermore, L, between Zn and O was determined for pure ZnO is in good agreement with reported Zn-O bond which is 1.9767 Å [45]. However, for Ce doped ZnO nanorods, L are slightly different from pure Zn-O. The slight change emphasized that Ce dopant has moderately affected ZnO lattice structure.

Fig. 2 shows the surface morphology of as-synthesized samples which clearly have the wurtzite hexagonal structure. The measured diameter and the length of the nanorods were in the range 100 - 150 nm and 1 - 1.5 μm, respectively. As evidenced in Fig. 2, ZnO maintains its hexagonal structure up to higher percentages of Ce-doping and no morphological change was observed.

4.2. Energy dispersive X-ray spectroscopy

Fig. 3 shows EDX spectra of as-synthesized samples with different levels of doping (0.0, 6.0, 8.0 and 10.0 at% Ce, respectively). EDX spectra for sample at 4.0 at% Ce not shown here, because spectra is similar for undoped sample. Sharp peaks of Zn and O were observed in the EDX spectra. However, very small peaks were detected for Ce at higher doping percentage (Fig. 3 c and d). This indicates that Ce has been incorporated successfully into the ZnO lattice. EDX results are in good agreement with XRD. Furthermore, peaks related to Na, Si, Sn and In were also seen and can be assigned to the ITO glass substrate.

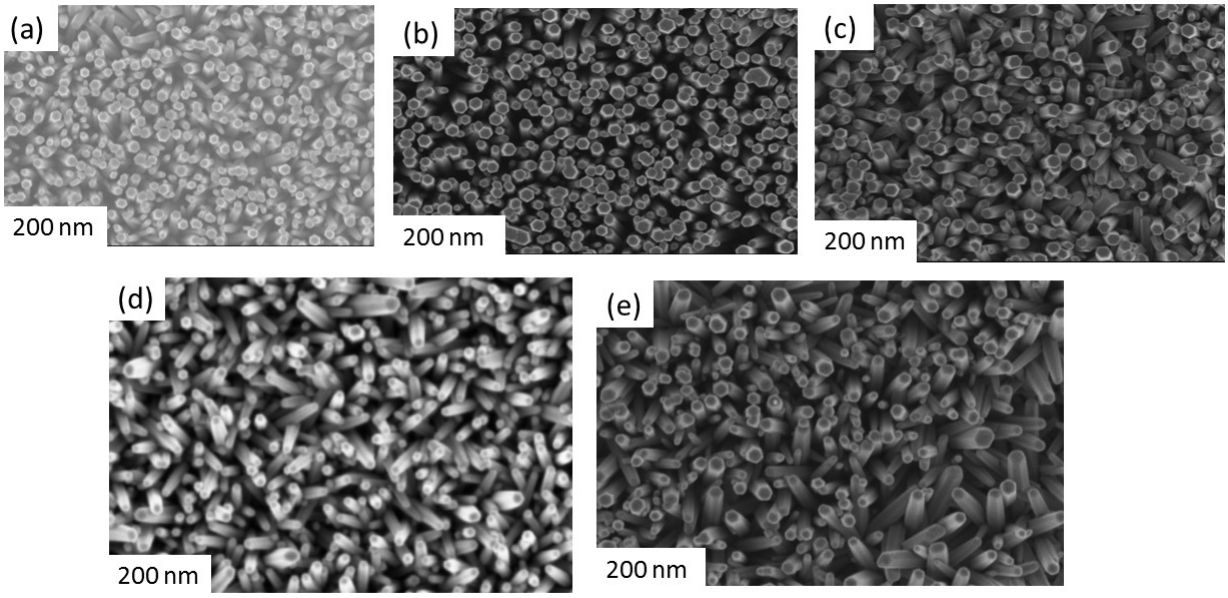

Figure 2: FESEM images of as-synthesized samples. (a) 0.0, (b) 4.0, (c) 6.0, (d) 8.0 and (e) is 10.0 at% Ce doped ZnO nanorods, respectively. The insets shows they area in which the spectra was acquired.

4.3. Optical properties

4.3.1. Raman Spectroscopy

Raman scattering is known for its sensitivity to the nanostructured materials and can be used to yield information about phase purity and crystallinity of as-synthesized samples. Fig. 4 (A) shows room temperature Raman spectra of the undoped and Ce doped ZnO nanorods in the range 150 to 1500 cm^{-1} excited by a 532 nm laser. At the center of the Brillouin zone (Γ point) the optical phonons are involved in the first order Raman scattering and according to group theory the following lattice optical phonons exist:

$$\Gamma_{Optical} = A_1 + E_1 + 2B_1 + 2E_2 \tag{1}$$

B_1, A_1 and E_1 are the silent modes and the first order Raman active modes, respectively, as stated by the Raman selection rule. The A_1 and E_1 are polar Raman and infrared active modes, and they split into transverse optical (TO) and longitudinal optical (LO) phonons. E_2 is nonpolar mode and splits into high and low frequency phonons. The observed peaks in Raman spectra can be assigned to the ZnO wurtzite structure lattice vibration with space group $C^4_{6v}(P6_3mc)$ [46]. Observed peaks at 333 cm^{-1} and 339 cm^{-1} are allocated to E_2 high - E_2 low and E_2 high modes, respectively. The appearance of E_2 high as a dominant peak over the E_2 low peak indicated that samples with good quality have been synthesized which is in good agreement with XRD results presented in section 4.1. It can be noted from Fig. 4 (B) that, the E_2 high peaks shifted to higher wavenumber when the Ce dopant content is increased compared to the undoped ZnO nanorods. Observed peak at 579 cm^{-1} is assigned to A_1 LO mode and it is due to defects present in the samples [47] such as oxygen vacancies due to the Ce-doping in ZnO nanorods. Furthermore, the broad peak between 1050 cm^{-1} and 1200 cm^{-1} is attributed to the multiphonons $2E_1$(LO), $2A_1$ (LO) modes and it is a characteristic feature of II - VI semiconductors [46, 48, 49].

4.3.2. Photoluminescence

Fig. 5 shows room temperature photoluminescence (PL) of undoped and Ce doped ZnO nanorods from 0.0 to 10.0 at% Ce measured with excitation wavelength 344 nm. Two main emission peaks are observed in PL spectra

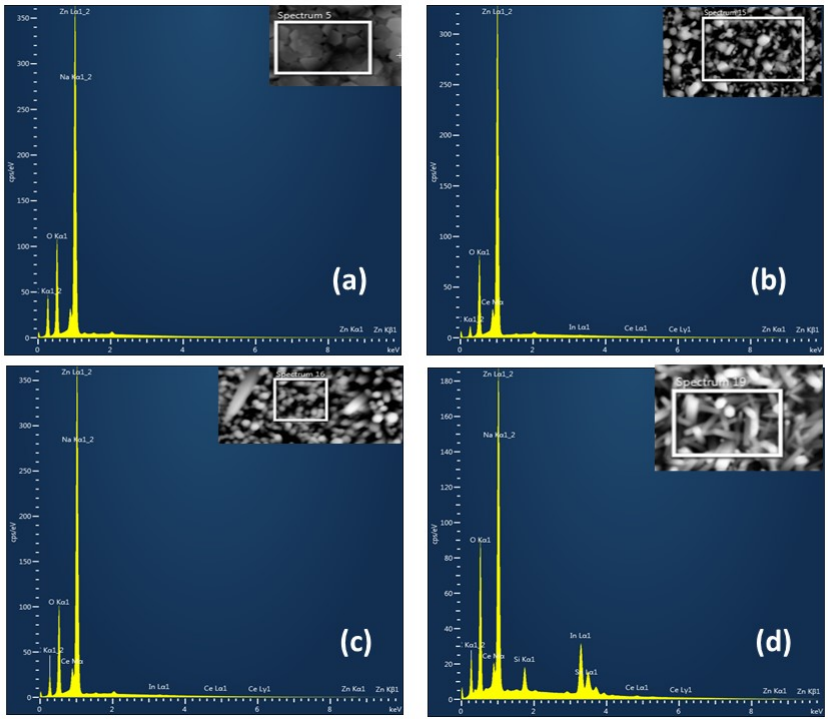

Figure 3: EDX spectra of (a) 0.0, (b) 6.0, (c) 8.0 and (d) is 10.0 at% Ce, respectively. The insets shows the area in which the spectrum was taken.

namely, UV and visible light as depicted in Fig. 5 (A) and 5 (B), respectively. The UV peaks of pure and Ce doped ZnO nanorods with various levels of doping (0.0, 4.0, 6.0, 8.0 and 10.0) at% Ce are positioned at 403 nm, 404 nm, 404 nm, 407 nm and 405.00 nm, respectively. The UV emission is also known as near band edges emission and originates from the free exciton recombination of ZnO through exciton-exciton collisions [50, 51, 52]. After the Ce dopant is introduced and incorporated into the ZnO lattice, it is expected that the band structure of ZnO will be altered significantly, and new emission will be established. It can be observed from PL spectra that the UV peaks of Ce doped ZnO nanorods are red shifted with respect to undoped ZnO nanorods. This shift may be due to the replacement of Zn^{+2} by Ce^{+3}/Ce^{+4} in ZnO lattice and because of the electron localizations of Ce, impurity bands (electron states) will be introduced. These impurity bands will be located near to the conduction band (lower edges), resulting in a formation of unoccupied band which in turn reduces the band gap and eventually causes the red shift of the UV peak [53]. The shift in the UV peak position is compatible with E_2 high Raman shift described in section 4.3.1. The UV emission also shows small peaks located at 388. These peaks may be attributed to the energy transition in ZnO between an electron in Zn interstitial defect states and a hole in the valence band. Similar behaviour has been reported in Sm doped ZnO nanorods [54]. PL spectra of pure and Ce doped ZnO nanorods also show blue emission peak located at 470 nm and may originate from recombination of the Zn 4p and O 2p electrons in the conduction and valence band, respectively [39].

The broad emission peak in the green-yellow region of the visible light spectrum is attributed to deep-level emission and is due to different point defects, such as oxygen vacancy, zinc interstitial and surface defect [39, 55, 56, 57, 58]. As seen in Fig. 5 (B), the green-yellow emission is initially enhanced compared to pure ZnO when Ce dopant is introduced, reaching a maximum emission for 4.0 at% Ce. Further increase in Ce dopant concentrations resulted in a decrease in the intensity of the green-yellow emission. Introducing more dopant can increase the defects in the sample, possibly oxygen vacancies. The decrease in the emission intensity at higher concentration could be due to the formation of defects in the sample, which results in increasing scattering of the photons. Similar phenomena were observed for N-doped ZnO nanorods arrays [59]. Mahmood et al. [59] found that the PL peak intensity decreased at

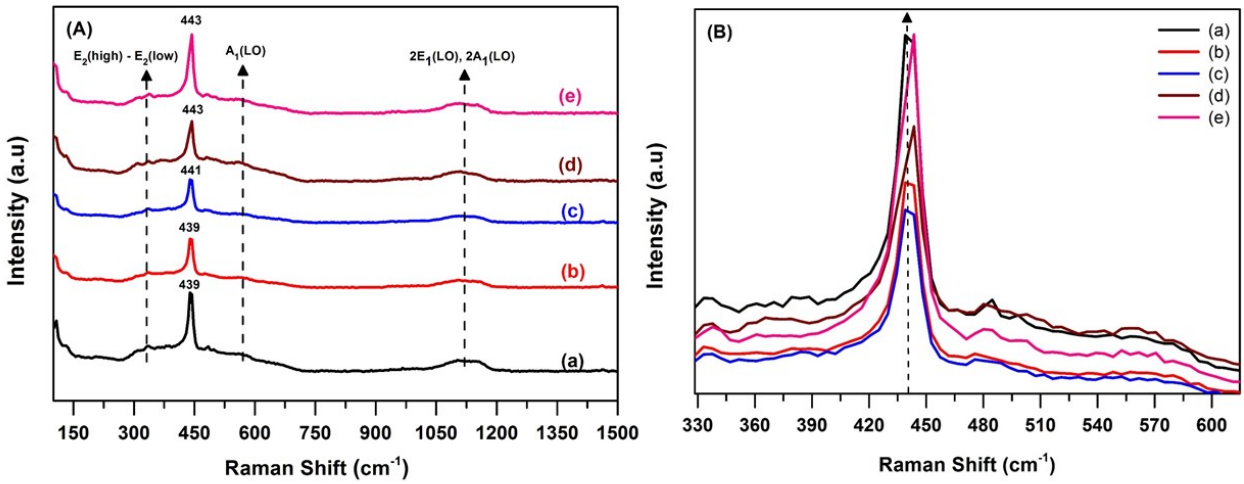

Figure 4: (Color online) (A) Room temperature Raman spectra (Y-Offset) of undoped and Ce doped ZnO nanorods at different levels of doping: (a) 0.0, (b) 4.0, (c) 6.0, (d) 8.0 and (e) is 10.0 at% Ce, respectively. (B) The E_2 (high) mode showing the shift in the peak with increasing the Ce dopant.

higher levels of N dopant due to increased photon scattering by defect caused by doping in the crystal. The presence of defects seen by PL are in good agreement with results from Raman scattering (see Fig. 4).

4.3.3. UV-vis

Fig. 6 shows room temperature UV-vis transmittance spectra of pure and Ce doped ZnO nanorods. After the initial drop at 4.0 at% Ce, the overall transmittance in the visible region first increased and then decreased with increasing Ce concentrations and shows maximum at 10.0 at% Ce ($\approx$ 81.3 %) doped ZnO nanorods. As on can observe in the range of 500 - 800 nm the optical transmittance decreased from 75.5% at 0.0 at% Ce to 68% at 4.0 at% and thereafter, it increased to 78.9% at 6.0 before it decreased again to 74.0 % at 8.0 at% Ce. Finally the transmittance increased to 81.3 % at 10.0 at% Ce. Similar trends have also been reported for Ce and Sm doped ZnO [38, 60]. It can be seen from Fig. 6, pure and Ce doped ZnO nanorods do not transmit the UV light below 300 nm. The presence of a broad peak in the range of 300 - 315 nm and it become more pronounced for Ce doped ZnO nanorods at 6.0 at% could be due the defect presented in the nanorods.

The optical band gap (E_g) of a direct band gap ZnO wurtzite structure was calculated using Tauc's law [61]:

$$(\alpha h\nu)^2 = C^*(h\nu - E_g) \tag{2}$$

where, $h\nu$ is the phonon energy, C^* is constant, E_g is the optical energy gap and α is the absorption coefficient calculated using equation [61]:

$$\alpha = (\frac{1}{d})\ln(\frac{1}{T}) \tag{3}$$

where d represents the thickness of the nanorods and T is transmittance. The optical band gap was extracted from the Tauc's plot ($(\alpha h\nu)^2$ versus $h\nu$) in which straight line portion was extrapolated to zero absorption coefficients ($\alpha = 0$) as shown in Fig. 7 (plot not shown for 4.0 at% Ce). The obtained E_g values for, 0.0, 4.0, 6.0, 8.0 and 10.0 at% Ce doped

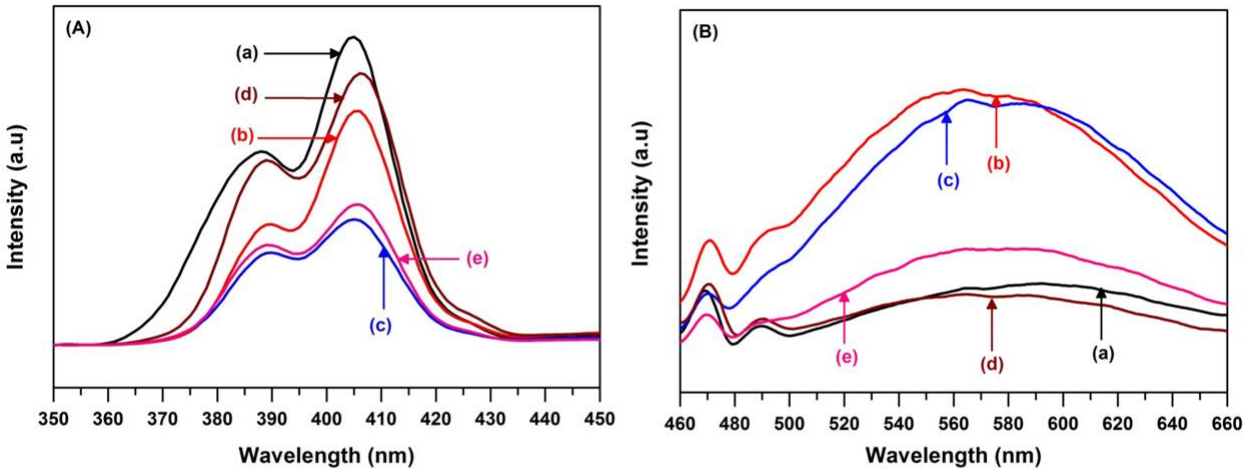

Figure 5: (Color online) PL spectra of (a) 0.0, (b) 4.0, (d) 6.0, (c) 8.0 and (f) is 10.0 at% Ce doped ZnO nanorods, respectively, measured at room temperature. (A) and (B) are the UV and the green-yellow emission, respectively.

ZnO nanorods were 3.240, 3.236, 3.267, 3.290 and 3.288 eV, respectively. The E_g value increased with increasing Ce dopant concentration when compared to undoped ZnO nanorods. This widening in the optical band gap could be due to the well known Moss-Burstein effect [62, 63, 64].

4.4. Electrical characterization

Fig. 8 shows forward and reverse bias semilogarithmic *I-V* characteristics of Pd/ZnO/ITO Schottky diodes based on pure and Ce doped ZnO nanorods measured at room temperature. The structures have exhibited an excellent rectification behaviour when ZnO was doped with Ce, as shown in Fig. 8. It should be mentioned that, the Pd contacts were annealed in air at 300° C for 3 min. The fabricated nanorods of pure and Ce doped ZnO underneath the Pd contacts could be considered as a collections of a single Schottky diodes aligned together in parallel. As evidenced in Fig. 8, the rectification is significantly improved by increasing the Ce dopant at the applied voltages -1 V. The difference between forward and reverse bias at 10.0 at% Ce doped ZnO nanorods is six orders of magnitude compared to the pure sample (see Fig. 8). Obtained results for Schottky diodes at 0.0 at% Ce are similar to our previous work doping with Sm [54].

The *I-V* characteristics in Fig. 8 can be divided into three regions: the reverse bias (I), the thermionic emission (II) and the series resistance limited region (III). The thermionic emission region increase in width and the linear section become steeper with addition of Ce compared to the undoped diodes. Further increase in the Ce dopant does not change the linearity of *I-V* plot. However, increasing the Ce dopant increase the series resistance. The *I-V* characteristics of Schottky diode forward bias can be described using the thermionic emission theory [65].

The observed values of the Schottky barrier height, ideality factor and the saturation current as determined from the fit are shown in Table 2. The obtained n values are slightly higher than the value for an ideal diode ($n = 1$) which may be ascribed to some factors such as surface and interface states, series resistance, voltage drop across the metal semiconductor junction and interfacial dielectric layers [66, 67].

The obtained Schottky barrier height from the fit at applied zero voltage for undoped samples deviated from the theoretically calculated one $\approx$ 1.0 eV (difference between the Pd work function (5.22 eV) and ZnO electron affinity

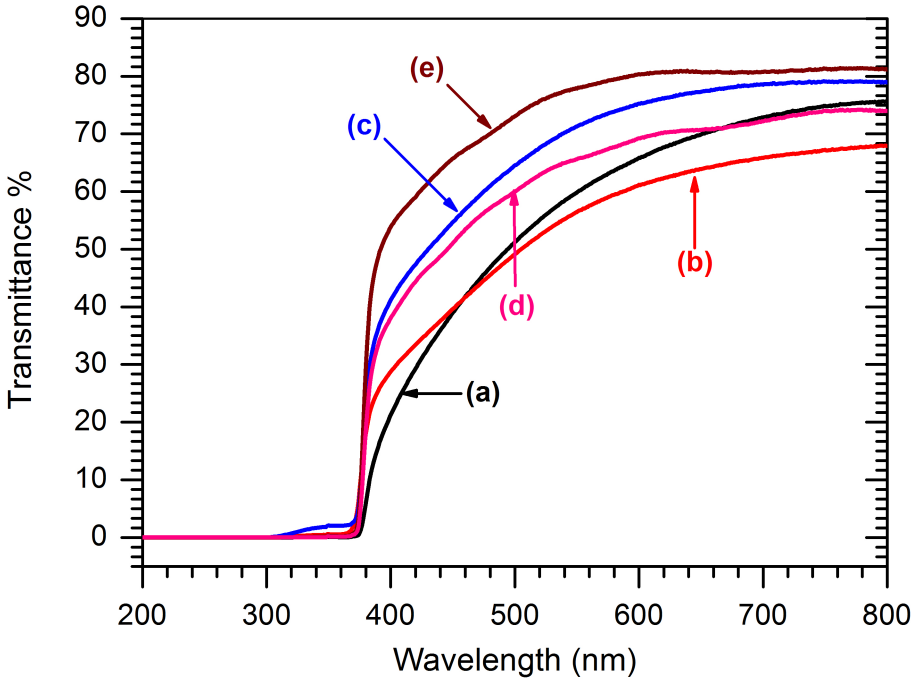

Figure 6: (Color online) The UV-vis transmittance spectra of pure and Ce doped ZnO nanorods: (a) 0.0, (b) 4.0, (c) 6.0, (d) 8.0 and (e) is 10.0 at% Ce, respectively, measured at room temperature.

Table 2: Schottky barrier height, ideality factor and saturation current of a fabricated Schottky devices based on Ce doping in ZnO nanorods.

Concentration (at%)	ϕ_B (eV)	n	I_s (Amps)
0.0	0.553	4.45	79.13×10^{-8}
4.0	0.764	3.00	12.64×10^{-11}
6.0	0.826	1.36	9.10×10^{-12}
8.0	0.824	1.37	23.12×10^{-12}
10.0	0.856	1.34	3.43×10^{-12}

(4.20 eV)). However, for Ce doped samples the deviation is less than for the undoped samples. This deviation could be due to the formation of barrier height inhomogeneities at the interface resulting in deviation from linearity of *I-V* characteristics [68] or the presence of interface states.

Fig. 8 also shows that the increase in reverse bias current (region I) with increasing applied reverse voltage becames more pronounced for Ce doped ZnO samples. This increase in the reverse current may be attributed to the presence of an insulator layer between metal and semiconductor, inhomogeneity of barrier height and image force effect [68]. It can also be observed from Fig. 8 that, the series resistance denoted by region III at 8 at% is higher compared to the rest of the samples. This could be due the formation of poor contact between the Pd and the nanorods.

5. Conclusion

In summary, Schottky diodes based on pure and Ce doped ZnO nanorods were fabricated on ITO substrates using a chemical bath deposition technique. XRD results revealed that the as-synthesized samples were highly crystalline

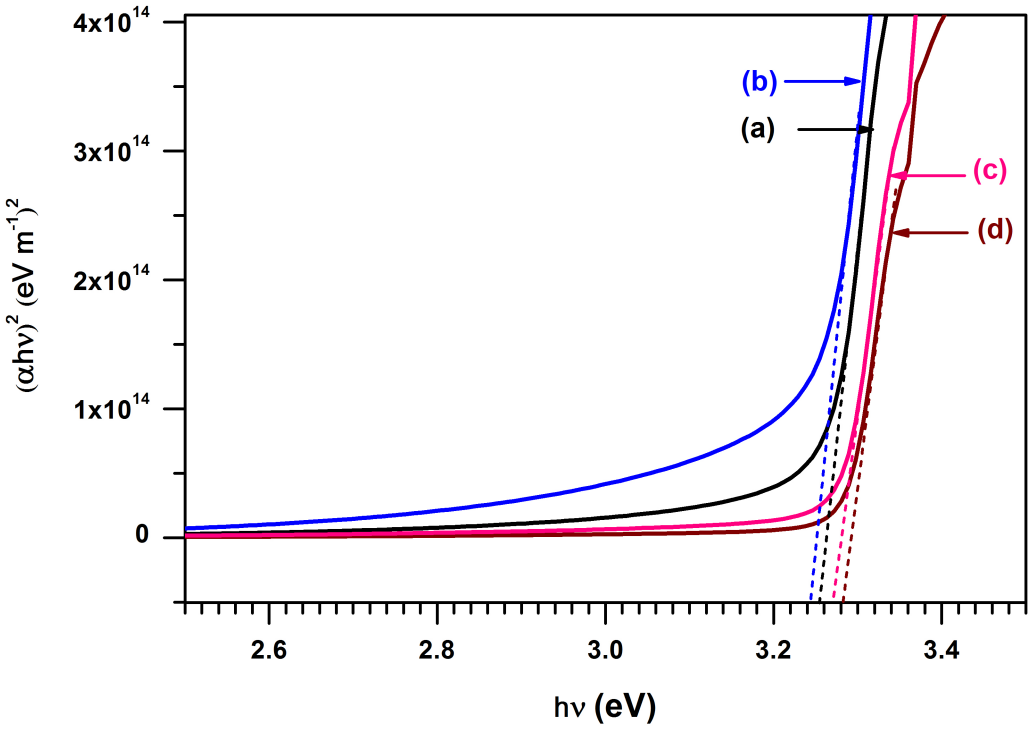

Figure 7: (Color online) Tauc's plot of (a) 0.0, (b) 6.0, (c) 8.0 and (d) is 10.0 at% Ce doped ZnO nanorods, respectively.

nanorods grown perpendicularly to the ITO substrate. Moreover, no other peaks except those due to ZnO and the ITO substrates were observed, indicating that the Ce has been successfully incorporated into the ZnO lattice. Raman spectra showed a sharp and intense E_2 high mode, indicating that the ZnO was highly crystalline with a wurtzite structure. The E_2 high mode peak was red shifted with increasing the Ce dopant concentrations. The PL spectra measured at room temperature showed two main peaks namely, a UV and a green-yellow band in the visible region. The PL spectra also revealed small UV peaks located at 388 and 393 nm. Furthermore, Ce doping in ZnO nanorods enhanced the green-yellow emission. The optical band gap obtained from UV-vis results indicated that Ce has increased the optical band gap. The electrical characterization of the Schottky diodes were investigated by *I-V* measurements at room temperature, and the electrical parameters were determined. The rectification behaviour of the Schottky diodes was improved by increasing the Ce dopant concentrations with maximum rectification attained at 10.0 at% Ce with barrier height and ideality factor of 0.856 eV and 1.34, respectively.

Acknowledgment

This work is supported by the South African Research Foundation (NRF) grant no: 91550 and 111 744. The opinions, findings and conclusion are those of the authors and the NRF accepts no responsibility whatsoever in this regard. The authors would like to thank Dr. Shankara, from the department of Chemistry at the University of Pretoria for the UV-vis measurements and the authors also wish to thanks Prof. Hendrik Swart, from the department Physics at the University of Free State for XRD and PL measurements.

References

[1] J. G. Lu, P. Chang, Z. Fan, Quasi-one-dimensional metal oxide materialssynthesis, properties and applications, Mater. Sci. Eng. R Rep. 52 (1) (2006) 49–91.

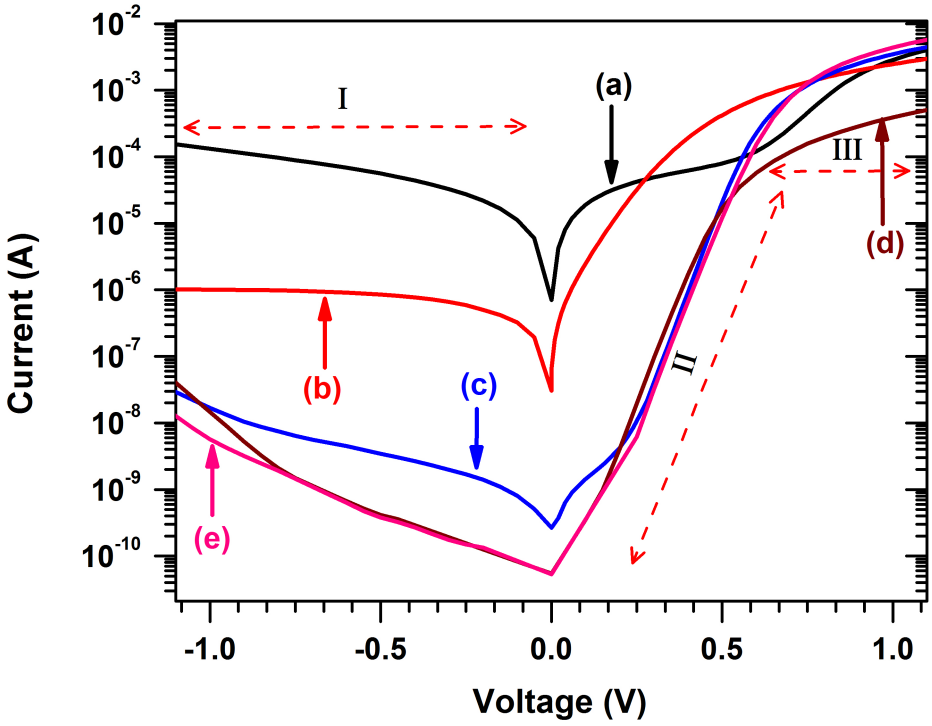

Figure 8: (Color online) Room temperature *I-V* characteristics of undoped and Ce doped ZnO nanorods at different concentrations: (a) 0.0 , (b) 6.0, (c) 8.0 and (d) is 10.0 at% Ce, respectively.

[2] J. Hu, T. W. Odom, C. M. Lieber, Chemistry and physics in one dimension: synthesis and properties of nanowires and nanotubes, Accounts of chemical research 32 (5) (1999) 435–445.

[3] Y. Cui, C. M. Lieber, Functional nanoscale electronic devices assembled using silicon nanowire building blocks, Science 291 (5505) (2001) 851–853.

[4] P. Yang, H. Yan, S. Mao, R. Russo, J. Johnson, R. Saykally, N. Morris, J. Pham, R. He, H. Choi, et al., Controlled growth of ZnO nanowires and their optical properties, Adv. Funct. Mater. 12 (5) (2002) 323–331.

[5] Z. Dai, Z. W. Pan, Z. L. Wang, Novel nanostructures of functional oxides synthesized by thermal evaporation, Adv. Funct. Mater. 13 (1) (2003) 9–24.

[6] J. Müller, S. Weissenrieder, ZnO-thin film chemical sensors, Fresenius J. Analy. Chemi. 349 (5) (1994) 380–384.

[7] T. H. Lee, H. J. Sue, X. Cheng, ZnO and conjugated polymer bulk heterojunction solar cells containing ZnO nanorod photoanode, Nanotechnology 22 (28) (2011) 285401.

[8] W. C. Shih, M. S. Wu, Growth of ZnO films on GaAs substrates with a SiO_2 buffer layer by RF planar magnetron sputtering for surface acoustic wave applications, J. Cryst. Growth 137 (3) (1994) 319–325.

[9] M. Nistor, E. Millon, C. Cachoncinlle, W. Seiler, N. Jedrecy, C. Hebert, J. Perrière, Transparent conductive Nd-doped ZnO thin films, J. Phys. D: Appl. Phys. 48 (19) (2015) 195103.

[10] Y. W. Song, K. Kim, J. P. Ahn, G. E. Jang, S. Y. Lee, Physically processed Ag-doped ZnO nanowires for all-ZnO p–n diodes, Nanotechnology 20 (27) (2009) 275606.

[11] Y. Li, X. Zhao, W. Fan, Structural, electronic, and optical properties of Ag-doped ZnO nanowires: first principles study, J. Phys. Chem. C 115 (9) (2011) 3552–3557.

[12] M. Yan, H. Zhang, E. Widjaja, R. Chang, Self-assembly of well-aligned gallium-doped zinc oxide nanorods, J. Appl. Phys. 94 (8) (2003) 5240–5246.

[13] H. Wang, S. Baek, J. Song, J. Lee, S. Lim, Microstructural and optical characteristics of solution-grown Ga-doped ZnO nanorod arrays, Nanotechnology 19 (7) (2008) 075607.

[14] V. Roy, A. Djurišić, H. Liu, X. Zhang, Y. Leung, M. Xie, J. Gao, H. Lui, C. Surya, Magnetic properties of Mn doped ZnO tetrapod structures, Appl. Phys. lett. 84 (5) (2004) 756–758.

[15] H. Yan, X. Zhong, J. Wang, G. Huang, S. Ding, G. Zhou, Y. Zhou, Cathodoluminescence and room temperature ferromagnetism of Mn-doped ZnO nanorod arrays grown by chemical vapor deposition, Appl. Phys. lett. 90 (8) (2007) 082503.

[16] Y. Kim, W. Tai, Electrical and optical properties of Al-doped ZnO thin films by sol–gel process, Appl. Surf. Sci. 253 (11) (2007) 4911–4916.
[17] P. VM, S. B. V, K. Balakrishna, K. Naik, Deposition of undoped and Al doped ZnO thin films using RF magnetron sputtering and study of their structural, optical and electrical properties, AIP Conf. Proc. 1832 (1) (2017) 080041.
[18] W. I. Park, D. H. Kim, S. W. Jung, G. C. Yi, Metalorganic vapor-phase epitaxial growth of vertically well-aligned ZnO nanorods, Appl. Phys. Lett. 80 (22) (2002) 4232–4234.
[19] B. D. Yao, Y. F. Chan, N. Wang, Formation of ZnO nanostructures by a simple way of thermal evaporation, Appl. Phys. Lett. 81 (4) (2002) 757–759.
[20] D. H. Zhang, Z. Y. Xue, Q. P. Wang, The mechanisms of blue emission from ZnO films deposited on glass substrate by rf magnetron sputtering, J. Phys. D: Appl. Phys. 35 (21) (2002) 2837–2840.
[21] J. H. Choi, H. Tabata, T. Kawai, Initial preferred growth in zinc oxide thin films on Si and amorphous substrates by a pulsed laser deposition, J. Cryst. Growth 226 (4) (2001) 493–500.
[22] M. G. Ambia, M. N. Islam, M. O. Hakim, The effects of deposition variables on the spray pyrolysis of ZnO thin film, J. Mater. Sci. 29 (24) (1994) 6575–6580.
[23] N. Saito, H. Haneda, T. Sekiguchi, N. Ohashi, I. Sakaguchi, K. Koumoto, Low-temperature fabrication of light-emitting zinc oxide micropatterns using self-assembled monolayers, Adv. Mater. 14 (6) (2002) 418–421.
[24] N. Fifere, A. Airinei, D. Timpu, A. Rotaru, L. Sacarescu, L. Ursu, New insights into structural and magnetic properties of Ce doped ZnO nanoparticles, J. Alloys Compd. 757 60–69.
[25] J. Sin, S. Lam, K. Lee, A. R. Mohamed, Preparation and photocatalytic properties of visible light-driven samarium-doped ZnO nanorods, Ceram. Int. 39 (5) (2013) 5833–5843.
[26] P. Velusamy, R. R. Babu, K. Aparna, Effect of Sm doping on the physical properties of ZnO thin films deposited by spray pyrolysis technique, in: AIP Conf. Proc., Vol. 1832, AIP Publishing, 2017, p. 080085.
[27] O. Lupan, T. Pauporte, B. Viana, P. Aschehoug, M. Ahmadi, B. R. Cuenya, Y. Rudzevich, Y. Lin, L. Chow, Eu-doped ZnO nanowire arrays grown by electrodeposition, Appl. Surf. Sci. 282 (2013) 782–788.
[28] P. Korake, A. Kadam, K. Garadkar, Photocatalytic activity of Eu $^{3+}$-doped ZnO nanorods synthesized via microwave assisted technique, J. Rare Earths 32 (4) (2014) 306–313.
[29] M. Najafi, H. Haratizadeh, M. Ghezellou, The effect of annealing, synthesis temperature and structure on photoluminescence properties of Eu-doped ZnO nanorods, J. Nanostruct. 5 (2) (2015) 129–135.
[30] M. Balestrieri, G. Ferblantier, S. Colis, G. Schmerber, C. Ulhaq-Bouillet, D. Muller, A. Slaoui, A. Dinia, Structural and optical properties of Yb-doped ZnO films deposited by magnetron reactive sputtering for photon conversion, Sol. Energy Mater. Sol. Cells 117 (2013) 363–371.
[31] R. Zamiri, A. Lemos, A. Reblo, H. A. Ahangar, J. Ferreira, Effects of rare-earth (Er, La and Yb) doping on morphology and structure properties of ZnO nanostructures prepared by wet chemical method, Ceram.s Int. 40 (1) (2014) 523–529.
[32] A. J. Kulandaisamy, V. Elavalagan, P. Shankar, G. K. Mani, K. J. Babu, J. B. B. Rayappan, Nanostructured cerium-doped ZnO thin film–A breath sensor, Ceram. Int. 42 (16) (2016) 18289–18295.
[33] J. Lang, J. Wang, Q. Zhang, X. Li, Q. Han, M. Wei, Y. Sui, D. Wang, J. Yang, Chemical precipitation synthesis and significant enhancement in photocatalytic activity of Ce-doped zno nanoparticles, Cer. Int. 42 (12) (2016) 14175–14181.
[34] A. Chelouche, T. Touam, M. Tazerout, D. Djouadi, F. Boudjouan, Effect of Li codoping on highly oriented sol-gel Ce-doped ZnO thin films properties, J. Lumin. 188 (2017) 331–336.
[35] D. Gao, L. Lyu, B. Lyu, J. Ma, L. Yang, J. Zhang, Multifunctional cotton fabric loaded with Ce doped ZnO nanorods, Mater. Res. Bull 89 (2017) 102–107.
[36] C. Ge, C. Xie, S. Cai, Preparation and gas-sensing properties of Ce-doped ZnO thin-film sensors by dip-coating, Mate. Sci.Eng.: B 137 (1-3) (2007) 53–58.
[37] G. Dar, A. Umar, S. Zaidi, A. Ibrahim, M. Abaker, S. Baskoutas, M. Al-Assiri, Ce-doped ZnO nanorods for the detection of hazardous chemical, Sens. Actuators B 173 (2012) 72–78.
[38] M. Yousefi, M. Amiri, R. Azimirad, A. Z. Moshfegh, Enhanced photoelectrochemical activity of Ce doped ZnO nanocomposite thin films under visible light, J. Electroanal Chem. 661 (1) (2011) 106–112.
[39] M. Elias, M. Amin, S. Firoz, M. A. Hossain, S. Akter, M. A. Hossain, M. Uddin, I. Siddiquey, Microwave-assisted synthesis of Ce-doped ZnO/CNT composite with enhanced photo-catalytic activity, Ceram. Int. 43 (1) (2017) 84–91.
[40] C. Chang, C. Lin, M. Hsu, Enhanced photocatalytic activity of Ce-doped ZnO nanorods under UV and visible light, J. Taiwan Inst. Chem. Engineers 45 (4) (2014) 1954–1963.
[41] N. Sinha, G. Ray, S. Bhandari, S. Godara, B. Kumar, Synthesis and enhanced properties of cerium doped ZnO nanorods, Ceram. Int. 40 (8) (2014) 12337–12342.
[42] U. Holzwarth, N. Gibson, The scherrer equation versus the'Debye-Scherrer equation', Nat. Nanotechnol. 6 (9) (2011) 534–534.
[43] G. Murtaza, M. A. Iqbal, Y. B. Xu, I. G. Will, Z. C. Huang, Study of Sm-doped ZnO samples sintered in a nitrogen atmosphere and deposited on n-si (1 0 0) by evaporation technique, J. Mag. Magn. Mater. 323 (24) (2011) 3239–3245.
[44] B. S. Mwankemwa, F. J. Nambala, F. Kyeyune, T. T. Hlatshwayo, J. M. Nel, M. Diale, Influence of ammonia concentration on the microstructure, electrical and raman properties of low temperature chemical bath deposited ZnO nanorods, Mater. Sci. Semicond. Process. 71 (2017) 209–216.
[45] U. Seetawan, S. Jugsujinda, T. Seetawan, A. Ratchasin, C. Euvananont, C. Junin, C. Thanachayanont, P. Chainaronk, Effect of calcinations temperature on crystallography and nanoparticles in ZnO disk, Mater. Sci. Appl. 2 (09) (2011) 1302.
[46] R. Cuscó, E. Alarcón-Lladó, J. Ibáñez, L. Artús, J. Jiménez, B. Wang, M. J. Callahan, Temperature dependence of Raman scattering in ZnO, Phys. Rev. B 75 (16) (2007) 165202.
[47] J. Yang, M. Gao, L. Yang, Y. Zhang, J. Lang, D. Wang, Y. Wang, H. Liu, H. Fan, Low-temperature growth and optical properties of Ce-doped ZnO nanorods, Appl. Surf. Sci. 255 (5) (2008) 2646–2650.
[48] J. N. Zeng, J. K. Low, Z. M. Ren, T. Liew, Y. F. Lu, Effect of deposition conditions on optical and electrical properties of ZnO films prepared by pulsed laser deposition, Appl. Surf. Sci. 197 (2002) 362–367.

[49] C. L. Du, Z. B. Gu, M. H. Lu, J. Wang, S. T. Zhang, J. Zhao, G. X. Cheng, H. Heng, Y. F. Chen, Raman spectroscopy of (Mn, Co)-codoped ZnO films, J. Appl. Phys. 99 (12) (2006) 123515.
[50] D. C. Reynolds, D. C. Look, B. Jogai, C. W. Litton, T. C. Collins, W. Harsch, G. Cantwell, Neutral-donor–bound-exciton complexes in ZnO crystals, Phys. Rev. B 57 (19) (1998) 12151.
[51] W. I. Park, Y. H. Jun, S. W. Jung, G. Yi, Excitonic emissions observed in ZnO single crystal nanorods, Appl. Phys. Lett. 82 (6) (2003) 964–966.
[52] D. Weissenberger, M. Dürrschnabel, D. Gerthsen, F. Pérez-Willard, A. Reiser, G. M. Prinz, M. Feneberg, K. Thonke, R. Sauer, Conductivity of single ZnO nanorods after Ga implantation in a focused-ion-beam system, Appl. Phys. Lett. 91 (13) (2007) 132110.
[53] A. Majid, A. Ali, Red shift of near band edge emission in cerium implanted GaN, J. Phys. D: Appl. Phys. 42 (4) (2009) 045412.
[54] M. A. M. Ahmed, B. S. Mwankemwa, E. Carleschi, B. P. Doyle, W. E. Meyer, J. M. Nel, Effect of Sm doping ZnO nanorods on structural optical and electrical properties of Schottky diodes prepared by chemical bath deposition, Mater. Sci. Semicond. Process. 79 (8) (2018) 53 – 60.
[55] B. K. Meyer, H. Alves, D. M. Hofmann, W. Kriegseis, D. Forster, F. Bertram, J. Christen, A. Hoffmann, M. Straßburg, M. Dworzak, et al., Bound exciton and donor–acceptor pair recombinations in ZnO, Phys. Status Solid. B 241 (2) (2004) 231–260.
[56] V. A. Fonoberov, A. A. Balandin, Origin of ultraviolet photoluminescence in ZnO quantum dots: Confined excitons versus surface-bound impurity exciton complexes, Appl. Phys. lett. 85 (24) (2004) 5971–5973.
[57] A. B. Djurišić, W. C. H. Choy, V. A. L. Roy, Y. H. Leung, C. Y. Kwong, K. W. Cheah, T. K. Gundu Rao, W. K. Chan, H. Fei Lui, C. Surya, Photoluminescence and electron paramagnetic resonance of ZnO tetrapod structures, Adv. Funct. Mater. 14 (9) (2004) 856–864.
[58] Y. W. Heo, D. P. Norton, S. J. Pearton, Origin of green luminescence in ZnO thin film grown by molecular-beam epitaxy, J. Appl. Phys. 98 (7) (2005) 073502.
[59] K. Mahmood, S. B. Park, Growth and conductivity enhancement of N-doped ZnO nanorod arrays, J. Cryst. Growth 347 (1) (2012) 104–112.
[60] H. Y. He, J. Fei, J. Lu, Sm-doping effect on optical and electrical properties of ZnO films, J. Nanostruct. Chem. 5 (2) (2015) 169–175.
[61] J. Chen, D. Chen, J. He, S. Zhang, Z. Chen, The microstructure, optical, and electrical properties of sol-gel-derived Sc-doped and Al-Sc co-doped ZnO thin films, Appl. Surf. Sci. 255 (23) (2009) 9413–9419.
[62] C. Wu, J. Shen, J. Ma, S. Wang, Z. Zhang, X. Yang, Electrical and optical properties of molybdenum-doped ZnO transparent conductive thin films prepared by dc reactive magnetron sputtering, Semicond. Sci. Techol. 24 (12) (2009) 125012.
[63] V. Kumari, V. Kumar, B. P. Malik, R. M. Mehra, D. Mohan, Nonlinear optical properties of erbium doped zinc oxide (EZO) thin films, Opt. Commun. 285 (8) (2012) 2182–2188.
[64] P. F. H. Inbaraj, J. J. Prince, Optical and structural properties of Mg doped ZnO thin films by chemical bath deposition method, J. Mater. Sci. Mater. Electron. 29 (2) (2018) 935–943.
[65] E. Rhoderick, R. Williams, M.-S. Contacts, 2nd edn, Clarendon, Oxford.
[66] N. S. Singh, L. Kumar, A. Kumar, S. Vaisakh, S. D. Singh, K. Sisodiya, S. Srivastava, M. Kansal, S. Rawat, T. A. Singh, et al., Fabrication of zinc oxide/polyaniline (ZnO/PANI) heterojunction and its characterisation at room temperature, Mater. Sci. Semicond. Process. 60 (2017) 29–33.
[67] L. J. Brillson, Y. Lu, ZnO Schottky barriers and ohmic contacts, J. Appl. Phys. 109 (12) (2011) 8.
[68] D. Korucu, T. S. Mammadov, Temperature-dependent current-conduction mechanisms in Au/n-InP Schottky barrier diodes (SBDs), J. Opto-electron. Adv. Mater. 14 (1) (2012) 41.